HHS Public Access

Author manuscript

Nat Struct Mol Biol. Author manuscript; available in PMC 2013 August 01.

Published in final edited form as:

Nat Struct Mol Biol. 2013 February ; 20(2): 159–166. doi:10.1038/nsmb.2473.

The voltage-dependent gate in MthK potassium channels is located at the selectivity filter

David J. Posson[1], **Jason G. McCoy**[1], and **Crina M. Nimigean**[1,2,3]

[1]Department of Anesthesiology, Weill Cornell Medical College, New York, NY, USA

[2]Department of Physiology and Biophysics, Weill Cornell Medical College, New York, NY, USA

[3]Department of Biochemistry, Weill Cornell Medical College, New York, NY, USA

Abstract

Understanding how ion channels open and close their pores is crucial for understanding their physiological roles. We used intracellular quaternary ammonium blockers to locate the voltage-dependent gate in MthK potassium channels from *Methanobacterium thermoautotrophicum* with electrophysiology and X-ray crystallography. Blockers bind in an aqueous cavity between two putative gates, an intracellular gate and the selectivity filter. Thus, these blockers directly probe gate location: an intracellular gate will prevent binding when closed, whereas a selectivity filter gate will always allow binding. A kinetic analysis of tetrabutylammonium block of single MthK channels combined with X-ray crystallographic analysis of the pore with tetrabutylantimony unequivocally determined that the voltage-dependent gate, like the C-type inactivation gate in eukaryotic channels, is located at the selectivity filter. State-dependent binding kinetics suggests that MthK inactivation leads to conformational changes within the cavity and intracellular pore entrance.

INTRODUCTION

Ion channel gating, the opening and closing of the pore, is central to the regulation of ion movement across biological membranes. For some K^+ channels the primary activation gate is thought to reside at the intracellular end of the pore as a hydrophobic constriction of transmembrane helices, also called the bundle-crossing gate[1]. This concept originated from groundbreaking channel block experiments using the giant squid axon[2,3] and was later refined by numerous studies of voltage-gated K^+ (Kv) channels[4–6] and crystallographic studies of prokaryotic channels[7–10].

To whom correspondence should be addressed: crn2002@med.cornell.edu and djp2003@med.cornell.edu.

ACCESSION CODES

Protein Data Bank: Models and structure factors for the MthK (S68H V77C) pore crystallized in the absence and presence of TBSb have been deposited under accession codes 4HYO and 4HZ3, respectively.

AUTHOR CONTRIBUTIONS

D.J.P. and C.M.N designed the research; D.J.P. acquired and analyzed single channel data; D.J.P and J.G.M. acquired and analyzed crystallographic data; D.J.P, J.G.M. and C.M.N. wrote the paper.

Kv channels also have a secondary gate, called the C-type inactivation gate, located within the selectivity filter at the extracellular end of the pore[11–16]. Though many types of studies have converged on the selectivity filter model for C-type inactivation gating, only a subset have investigated the gate location with a physical probe in order to assess the bundle-crossing gate. Specifically, quaternary ammonium blockers and N-type inactivation peptides block the pore cavity, located between the bundle-crossing and selectivity filter gates, in the inactivated state[17,18] and methanethiosulfonate reagents can react to cysteines inside the inactivated state cavity[19,20]. These studies indicate that C-type inactivation may involve conformational changes below the selectivity filter while keeping the activation gate open. Therefore, two distinct gates have been identified within Kv channel pores and may function in other K^+ channel families.

Several studies of ligand-gated K^+ channels have challenged the notion that related channel families share gating features with Kv channels[21–25]. In particular, the primary ligand-controlled gate has been proposed to lie at the selectivity filter, rather than at a cytoplasmic constriction. Further complications have arisen in the analysis of BK channels, which are gated both by ligand (Ca^{2+}) and voltage. Despite the similarity between BK and Kv channels, several studies have suggested that the activation gate lies within the selectivity filter[26–29]. Taken together, these studies raise questions about the origins and structural differences underlying these gating mechanisms.

The MthK channel is a model Ca^{2+}-activated K^+ channel related to BK channels, but without voltage-sensor domains[9,30–32]. Ca^{2+}-dependent gating of MthK[9,33] was proposed to occur at the intracellular end of the pore by the straightening of inner-helices to form a bundle-crossing[10], although MthK has only been crystallized in an open state[9,10,34]. Additionally, at positive voltages, MthK closes even in the presence of activating Ca^{2+}, a gating process that has been shown to depend on extracellular ion composition similar to C-type inactivation in Kv channels, and hence inferred to occur at the selectivity filter[35]. At this time however, the physical location of the gates in MthK have not been directly probed either structurally or functionally.

In this study, we set out to conclusively determine the location of the voltage-dependent MthK gate by analyzing state-dependent block in single-channel recordings. The use of quaternary ammonium blockers to analyze voltage-dependent gating can be ambiguous and model-dependent due to the fact that blocker binding is voltage-dependent. In MthK channels however, the voltage dependence from the blockers occurs over a different voltage range than the voltage dependence of gating. At negative potentials, blockers couple to permeant K^+ ions, which confer voltage dependence to open-channel block[36]. At positive potentials, open-channel block becomes voltage independent, critical in determining blocker kinetics during MthK gating and the location of the voltage-dependent gate.

We investigated the state-dependent microscopic block kinetics for tetrabutylammonium (TBA), tetrapentylammonium (TPA), benzyltributylammonium (bTBA), and N-(4-[benzoyl]benzyl)-N,N,N-tributylammonium (bbTBA). We found that voltage gating did not prevent channel block but modestly reduced the on-rate for all blockers. Therefore, the voltage-dependent (inactivation) gate is above the blocker binding-site at the selectivity

filter and the entrance to the pore may be slightly constricted during inactivation. Interestingly, the off-rates changed in a blocker-dependent manner during inactivation, likely reflecting structural changes below the selectivity filter that accompany voltage gating but do not prevent blocker access. Finally, an analysis of X-ray diffraction data from a MthK pore in the presence of tetrabutylantimony (TBSb) indicated the binding site is immediately below the selectivity filter, as observed in KcsA structural data[8,37–39]. State-independent access of blockers to this site directly confirmed that the MthK voltage gate is located at the selectivity filter.

RESULTS

We set out to directly identify the location of the MthK voltage gate using quaternary ammonium probes that bind within the aqueous cavity of K^+ channels and block the current[3,26,39–41]. If the binding-site is located beyond an ion channel gate, the channel has to open for the blocker to bind, a process called gated-access (Figure 1a). This corresponds to the intracellular-facing gate described for Kv channels. In particular cases, the channel cavity may allow intracellular gate closure with the blocker bound, thereby physically trapping it inside (Figure 1a)[3,6,38]. Alternatively, if the channel gate is at the selectivity filter, the blocker can bind to both closed and open states (Figure 1b), and blocker binding is characterized by state-independent access to the block-site.

We studied blocker state-dependent accessibility during voltage-dependent gating of MthK to determine the location of the gate. Above 50 mV, voltage leads to a reduction in open probability (Po) (Figure 1c), previously shown[35]. Charged blockers, such as quaternary ammonium ions, are known to block ion channels in a voltage-dependent manner, during voltage-dependent gating[3,26] as well as in the absence of gating[36,42]. In order to separate the two processes, we first analyzed the blocker voltage-dependence at voltages less than 50 mV, where there is no voltage gating (Figure 1c).

Microscopic block of open MthK

We measured MthK block by TBA, bTBA, and bbTBA (Figure 2a), using single-channel recordings in planar lipid bilayers under conditions that maximized open probability[43]. We first analyzed block of open MthK (−125 to 50 mV, Figure 1c). Typical currents with and without blockers are in Figure 2a. Excursions to the closed state in the control recording, called flickers, are very brief, infrequent, and become negligible at positive voltages (Supplementary Figure 1)[33].

Addition of blockers decreased Po by increasing the time spent in non-conducting states. bbTBA blocked with the highest affinity, followed by bTBA and TBA. This correlated with the hydrophobicity increase due to each additional benzyl-group in the blocker stucture (Figure 2a). A similar hydrophobicity-dependence of block has long been appreciated for other K^+ channels[3,40,41]. The difference in blocker affinities reflects a dramatic change in kinetics, with bbTBA inducing longer closings than the other blockers (Figure 2a).

To quantitatively analyze block kinetics, we used the QuB program. Control recordings were fit with a two-state model, yielding single-exponential fits to the open and closed dwell

time distributions (Figure 2b). Addition of blocker introduces an additional closed component, requiring a model with two non-conducting states (Scheme I, Figure 2b). Blocker on-rates were proportional to blocker concentration while off-rates were concentration-independent, consistent with the bimolecular association shown in Scheme I (Supplementary Figure 2). The dissociation constant of the blocker for the open-state (K_D^{open}) was calculated from these rate constants. We investigated next how these parameters (k_{on}, k_{off}, and K_D^{open}) varied with voltage by analyzing single-channel block kinetics between −125 and 50 mV.

Permeant ions knock off the blocker from its site

Block of open MthK decreased at negative membrane potentials due to an acceleration of blocker off-rate (as seen by the reduced block durations, Figure 3a). At negative potentials, the dissociation constants (K_D^{open}) decreased exponentially with voltage with similar slopes for all blockers, suggesting a common mechanism (Figure 3b, open symbols). Interestingly, at positive potentials, blocker dissociation constants (or affinities) were voltage-independent.

Voltage-dependent channel block has often been modeled as the charged blocker traversing a portion of the membrane electric field to reach its binding site[44]. The model predicts that voltage changes will always modify block, unlike the plateau observed at positive voltages (Figure 3b). Furthermore, our kinetic analysis showed that blocker on-rate was voltage independent and thus the voltage dependence of blocker affinity was exclusively from the off-rate (Supplementary Figure 3). This is consistent with a blocker ‘knock-off’ effect, first described by Armstrong[3], suggesting that the blocker voltage-dependence is not intrinsic but arises from coupling with permeant ions moving in the field.

Martínez-François and Lu formulated a model to describe how blocker voltage-dependence can arise from the blocker’s coupled movement with permeant ions rather than its intrinsic movement[36], a concept that has been occasionally explored[42,45–47]. In this model (Figure 3c), the charged blocker does not bind within the membrane electric field, but in close proximity (aqueous cavity) to the permeant ions in the filter. At negative voltages, electrostatic repulsion between blocker and permeant ions leads to permeant ion redistribution in the filter upon blocker binding, experimentally observed as voltage-dependence of block (Figure 3c, diagonal transition). At positive voltages, permeant ions are preferentially distributed farther from the blocker site, electrostatic repulsion is thus relieved, and channel block is no longer voltage-dependent (Figure 3c, horizontal transition). This model predicts a blocker dissociation constant containing a voltage-dependent and a voltage-independent term ($K_D^{open}(V)$, Equation 2).

The permeant-ion coupling model fits the voltage dependence of K_D^{open} for all three blockers (Figure 3b). At increasing negative voltages, the exponential term is dominant (Equation 2) and the blocker affinity decreases as the K^+ ions knock off the blocker from its site. At positive voltages, the exponential term is negligible and K_D^{open} becomes essentially voltage independent. Our analysis of block during inactivation ($V \geq 50$ mV, Figure 3B) is thus substantially simplified by the constraint that any voltage dependence in this range is due to gating.

State-dependent block during MthK voltage gating

In order to identify the location of the inactivation gate, we investigated how block was affected by voltage gating. We first measured a model-independent apparent dissociation constant, K_D^{ap} (Equation 3) for each blocker over the inactivation voltage range ($V \geq 50$ mV, Figure 3b). Surprisingly, the blockers exhibited opposite apparent affinity changes: inactivation decreased the apparent affinity for bTBA and bbTBA (increased K_D^{ap}) but increased the apparent affinity for TBA (decreased K_D^{ap}) (Figure 3b).

Next, we examined which mechanisms of state-dependent block (Figure 1) predict the observed apparent affinities (Figure 3b). If the voltage gate is at the bundle-crossing and blocker can only bind to the open state (Scheme IIA, Figure 4a), K_D^{ap} is predicted to increase with voltage according to $K_D^{ap} = \frac{K_D^{open}}{P_o^{control}}$ (Supplementary Note). This can explain the apparent affinity changes for bTBA and bbTBA but cannot describe the voltage-dependent decrease of K_D^{ap} for TBA (Figure 3b). The "trapping" version of gated-access, which allows for channel closing after the blocker binds (Scheme IIB, Figure 4a) can fit either an increase or a decrease in apparent affinity as the channel closes (Supplementary Note). The trapping model is therefore consistent with the observed apparent affinities for all blockers.

If the voltage gate is at the selectivity filter, the blockers have state-independent access to their site (Scheme III, Figure 4a) and they bind with two affinities, one for the open state and another for the inactivated state (K_D^{open} and K_D^{inact}). This model can also explain the observed apparent affinities for all blockers. Consequently, an analysis of K_D^{ap} (Figure 3b) cannot distinguish between blocker gated access (with trapping) and state-independent access and thus between a gate at the bundle crossing and one at the filter.

TBA block locates the voltage gate at the selectivity filter

Using the trend in apparent affinity for TBA, we were able to narrow down the mechanism of block to either the gated-access model with trapping (Scheme IIB) or the state-independent access model (Scheme III). In order to distinguish between these two possibilities and the different gate locations they predict, we analyzed TBA microscopic block kinetics during gating. Single channel kinetic data were acquired for a range of blocker concentrations and voltages for three independent bilayers (Figure 4b and Supplementary Figure 4). Data were globally fit to the three models (IIA, IIB, and III, Figure 4a). Scheme III, describing the state-independent access model, was the best fit to the data (solid black lines in Figure 4b), clearly superior to the blocker-trapping model (green dotted lines) at high concentrations of TBA and high voltages, as well as to the gated-access open-channel block model (red dashed lines). Dwell-time distributions from all conditions are in Supplementary Figure 4 and fit parameters from all datasets are in Supplementary Tables. Confirming the visually better fits, Scheme III log-likelihood values were higher. These results show that closure of the voltage gate does not prevent TBA binding.

With our analysis, we were able to establish TBA affinity to the non-conducting, inactivated state, a conformation difficult to probe directly. Using the block parameters from Scheme III

(Supplementary Table 3), we calculated the K_D^{open}, K_D^{inact}, and the predicted K_D^{ap} (Figure 4c, Equation 4, Methods). Unsurprisingly, the predicted apparent dissociation constant (K_D^{ap}) was indistinguishable from the values determined experimentally. The TBA dissociation constant for the open state (K_D^{open}) from Scheme III also agreed with the value determined in the absence of inactivation (black line and green dotted line). The TBA dissociation constant for the inactivated state (K_D^{inact}, black dashed line) was an order of magnitude smaller than K_D^{open}. Thus, TBA not only accesses both the open and inactivated states, but binds to the inactivated state an order of magnitude more strongly, unambiguously indicating that the voltage gate is above the blocker binding site, at the selectivity filter.

bTBA and bbTBA block supports state-independent access

Can bTBA and bbTBA also bind to the inactivated MthK pore? Figure 3b showed that unlike TBA, the apparent affinities for bTBA and bbTBA decreased as the MthK channel inactivated, suggesting perhaps a different mechanism. To investigate, we analyzed single-channel datasets acquired over a range of intracellular blocker concentrations and voltages for bTBA and bbTBA. We found that the state-independent access model (Scheme III) fits the data in all conditions, while the open channel block model (Scheme IIA) failed to fit the data at high levels of inactivation (Figure 5a). Dwell-time distributions from all experimental conditions are in Supplementary Figure 5 and 6 and fit parameters from three datasets each for bTBA and bbTBA for Schemes IIa and III are in Supplementary Tables.

Using the block parameters from Scheme III (Supplementary Table 3), we calculated K_D^{open}, K_D^{inact}, and predicted K_D^{ap} for bTBA and bbTBA (Figure 5b). K_D^{ap} and K_D^{open} values agreed with values determined experimentally. The dissociation constant for the inactivated state (K_D^{inact}) was an order of magnitude larger than K_D^{open} for bbTBA and only twice as large for bTBA. Thus, the decrease in apparent affinities for bTBA and bbTBA during inactivation is not due to gated access but results from lower affinities to the inactivated state.

We also attempted to fit these data to the blocker-trapping model (Scheme IIB), but the parameters describing trapping (between OB and IB) were not well constrained and gave inconsistent results from channel to channel (not shown). We concluded that these data were not optimal for evaluating this model, likely reflecting our conclusion that the blocker affinity to the inactivated state was less than the affinity to the open state. We also reasoned that if TBA does not get trapped inside the channel (as we showed above), then the larger blockers, bTBA and bbTBA, would likely not be trapped either. Consequently, the high quality fits to the state-independent access model argues that all three blockers can bind to the inactivated state, strongly supporting voltage-dependent gating at the selectivity filter.

Inactivation alters binding kinetics of each blocker

We have shown that three quaternary ammonium blockers bind differently to the open and inactivated states. We have also analyzed an additional blocker, tetrapentylammonium (TPeA), over a limited set of conditions (Methods, Supplementary Figure 7 and Supplementary Table 3) to supplement our analysis of blocker state-dependence. The

differences in microscopic block kinetics between open and inactivated states suggest underlying conformational changes in the MthK pore during voltage gating.

Inactivation decreased the on-rate constant for all four blockers by 50–75 % (Figure 6a). This suggests that the barrier the blocker has to cross to enter the channel pore is increased for the inactivated relative to the open state. On the other hand, inactivation modified the off-rate in a blocker-dependent manner (Figure 6b). For TBA, the off-rate decreased by more than an order of magnitude during inactivation, overwhelming the decrease in on-rate and accounting for the large increase in affinity (decrease in K_D) relative to the open state (Figure 6c). For TPeA, the off-rate was reduced by ~80 %, resulting in a small increase in affinity upon inactivation. For bTBA, the off-rate was essentially state-independent and the affinity change during inactivation was entirely a result of the decrease in on-rate. For bbTBA, the off-rate was increased by inactivation ~250 %, decreasing the affinity (increasing the K_D) relative to the open state. Therefore, both tetra-alkylammonium blockers, TBA and TPeA, bound more strongly to the inactivated state, whereas the blockers with attached benzyl-rings, bTBA and bbTBA, bound more strongly to the open state.

Blockers bind immediately below the selectivity filter

The results above strongly locate the voltage gate above the binding site for quaternary ammonium blockers in the MthK pore. The binding sites within other K^+ channels are known to be in the aqueous cavity[4,8]. However, in order to unequivocally locate the voltage gate, we attempted to directly observe bound blocker inside the open MthK pore using X-ray crystallography[34]. High blocker concentrations in the crystals (~10 mM) did not result in interpretable blocker density distinct from the densities observed in the blocker-free pore electron density maps. We concluded that either the blocker binding is highly disordered or that the occupancy of bound blocker is very low inside the crystal. This last possibility may arise from the detergent, precipitant, or other crystal properties that may antagonize blocker binding.

In order to maximize the likelihood of observing bound blocker even at low occupancy, we collected diffraction data from MthK pore crystals containing the heavy tetrabutylantimony, TBSb. We constructed multiple difference maps using several datasets from MthK-TBSb crystals and MthK-no-blocker crystals. Figure 7 shows an example $F_o^{TBSb} - F_o^{no\text{-}blocker}$ difference map contoured at 4.5 σ. A single difference peak was observed in the maps at a site below the selectivity filter that aligned perfectly with a previously modeled TBA binding site in KcsA[38]. The strength of this difference peak was consistent with very low blocker occupancy within the crystal. However, the agreement with previous crystallographic evidence using the closed KcsA channel strongly suggests a conserved quaternary ammonium binding-site immediately below the selectivity filter.

DISCUSSION

In the absence of activating Ca^{2+}, MthK channels were proposed to close at an intracellular-facing gate analogous to the bundle-crossing in the KcsA closed structure[10]. It was conceivable that voltage-dependent gating of MthK also occurs at this location. A previous report on MthK voltage-dependent gating though, demonstrated gating sensitivity to external

[K^+] and suggested that the voltage-dependence arises from ion-occupancy of the selectivity filter[35], similar to C-type inactivation in Kv channels. However, a coupling mechanism between selectivity filter and an intracellular-facing gate was also a possibility.

We used quaternary ammonium blockers as state-dependent accessibility probes to investigate the physical location of the voltage-dependent gate within the pore of MthK channels. Unlike related studies of Kv[5,6], BK[26–28], HCN[48], and CNG[21,49] channels, we exclusively used kinetic analysis of single-channel block to demonstrate that the voltage gate is at the selectivity filter.

Blocking studies of voltage-gated ion channels require careful consideration of voltage dependent contributions from the movement of charged blocker and the gating of the channel[3,26]. Numerous studies of BK channels, eukaryotic homologues of MthK channels, which have been proposed to gate at the selectivity filter, highlight these challenges. Aldrich and coworkers showed that BK channel block by bbTBA displayed a voltage dependence that appeared to be consistent with gated access but was shown to result from the charged blocker itself, eventually concluding that bbTBA had state-independent accessibility to the BK pore[26]. This interpretation was later questioned by a modeling study that agreed with the binding of bbTBA to closed BK channels but suggested that partial activation of BK was required for bbTBA binding[28]. These studies highlight the difficulty in dissecting voltage-dependent gates, state-dependent affinities (due to conformational changes), voltage-dependent affinities (due to permeant ion coupling), and possible coupling between two gates. In the case of MthK, we were able to separate voltage-dependent changes in blocker affinity due to permeant ions (at negative voltages) and voltage-dependent changes due to inactivation gating (at voltages above 50 mV) since we showed they occur over different voltage ranges. This was a major advantage in our modeling and interpretation of the data as we were able to assume that the blocker affinities to the open and inactivated states were voltage-independent during inactivation (50–125 mV).

For the MthK open-channel block data in this study, we characterized blocker on- and off-rates as a function of voltage and found that voltage-dependent block was almost entirely due to blocker knock-off. That is, the on-rates were essentially voltage-independent, likely reflecting the absence of a substantial voltage drop across the pore cavity below the selectivity filter. This is an important finding because it provides experimental evidence that the fractional voltage drop across the cavity is very small for MthK, consistent with evidence for CNG channels and calculations using continuum electrostatics[50,51]. Other channels with similarly large or larger intracellular cavities, such as BK[29,52], also likely focus the membrane electric field entirely across the selectivity filter.

We determined that blockers access the MthK cavity in both open and inactivated states. The analysis of several blocker molecules was crucial, as only TBA proved ideal in distinguishing between the state-independent access and the blocker-trapping models, which led to a definitive location of the gate. bTBA and bbTBA showed a reduced affinity to the inactivated state that compromised their utility in directly ruling out blocker trapping. We reasoned that these larger blockers were less likely to be trapped than the smaller TBA,

which we showed was not trapped. The block kinetics for all blockers tested were very well accounted for by state-independent access to the binding site.

Does inactivation involve changes in the K^+ channel beyond the narrow confines of the selectivity filter? From our kinetic analysis (Figures 4–6), we obtained blocker on- and off-rates to both open and inactivated MthK for four blockers (TBA, TPeA, bTBA, and bbTBA). To our knowledge, only one blocker affinity has been reported for an inactivated K^+ channel conformation[20]. The kinetic basis for state-dependent block ($K_D^{open} \neq K_D^{inact}$), summarized in Figure 6, suggests structural changes in MthK beyond the selectivity filter during voltage gating. The on-rates for all four blockers were lower in the inactivated than in the open state, suggesting they have reduced access to the inactivated pore. Perhaps a small narrowing at the entrance to the pore accompanies inactivation.

The state-dependence of blocker off-rate was blocker specific. The inactivated pore binds TBA and TPeA for longer (off rates are slower in the inactivated state), while the open pore binds bbTBA for longer (off-rates are faster in the inactivated state). bTBA was the only blocker for which the off-rate was state-independent. These changes contribute to the final state-dependent affinities (Figure 6C). In the absence of structural data, it is difficult to speculate why different blockers vary in their state-dependent off-rates. It is possible that a conformational change such as a rotation or tilt of inner helices occurs in the pore below the selectivity filter during inactivation. Perhaps this conformational change enhances or disrupts the blocker-specific hydrophobic contacts with the protein. Other studies have indicated that selectivity filter gating may induce changes in the channel cavity or intracellular entryway[20,27,29,53–55], and in Kv channels for example, this may be related to coupling mechanisms between two gates[19,56]. In the context of ligand-gated channels such as MthK, we speculate that changes between open and inactivated conformations may reflect the allosteric connection between cytoplasmic ligand-binding domains and a selectivity-filter gate.

The location of the quaternary ammonium binding-site within the pore of K^+ channels was previously modeled for the closed KcsA channel using X-ray crystallography[37–39]. Recently, a high-resolution structure of the isolated open MthK pore was solved[34]. Unfortunately, our attempts to co-crystallize the MthK pore with blockers did not result in convincing electron density for modeling blocker binding. The effort was salvaged using a heavy-atom TBA analog, TBSb[8], that established the binding location immediately below the selectivity filter with an electron density difference peak from a $F_o^{TBSb} - F_o^{no\text{-}blocker}$ map. Importantly, our fundamental conclusion that the gate is within the selectivity filter does not depend on a precise molecular model of blocker binding.

In summary, we explored voltage-dependent block of the model MthK K^+ channel by four quaternary ammonium ions. The voltage-dependence of open-channel block was consistent with a model of blocker coupling to permeant K^+ ions. TBA was an ideal probe for analyzing state-dependent block during voltage gating as the intrinsic voltage-dependence of the block occurred over a different voltage range than the voltage-induced changes in the inactivation gate of MthK. Kinetic analysis revealed that blockers could access both open and inactivated states, although with different affinities. These results suggested possible

structural changes in the pore below the selectivity filter but ruled out gated-access to the block site. Crystallographic evidence using TBSb supported the picture of blocker binding below the selectivity filter, further establishing the location of the voltage-dependent inactivation gate at the selectivity filter.

ONLINE METHODS

MthK purification and reconstitution

MthK channels were expressed, purified, and reconstituted into proteoliposomes using protocols described previously[33]. All reagents were from Sigma unless otherwise indicated. Channels were purified in protein buffer (100 mM KCl, 20 mM HEPES, pH 7.6), with 5 mM n-decyl-β-D-maltopyranoside (DM, Affymetrix) and reconstituted into liposomes of 3:1 POPE:POPG (Avanti Polar Lipids). Lipids were solubilized in reconstitution buffer (400 mM KCl, 5 mM N-methyl-D-glucamine, 10 mM HEPES, pH 7.6) with 34 mM CHAPS (Affymetrix). Liposomes were formed and detergents were removed by passing MthK and lipids (1–5 μg protein per mg lipid) over a 20 mL Sephadex G50-fine column (GE Healthcare) using reconstitution buffer. Eluted liposomes were flash frozen in liquid nitrogen, and stored at −80 °C.

MthK pore-only crystallization

The pore of MthK (wild type or S68H V77C) was isolated from the intracellular domains and crystallized as previously described[34]. Trypsin type I (Sigma, T8003) was added to purified MthK at 1:50 trypsin:MthK (wt:wt) for 2 hours. Trypsin inhibitor type II-O (Sigma, T9253) was added at 2:1 inhibitor:trypsin (wt:wt) and digested protein was purified on a Superdex 200 column using protein buffer with 5 mM DM. The 14.3 mL peak was purified with a second Superdex 200 column using crystallization buffer (100 mM KCl, 10 mM MOPS, pH 8.0) with 10 mM Anagrade LDAO (Affymetrix). Protein was concentrated to 15 mg mL^{-1} (assuming 1 OD_{280} = 1 mg mL^{-1}). Crystals formed at 20 °C in sitting drops of 1.5 μL protein mixed with 1.5 μL well. Well solution was 3.5 – 4.0 M 1,6-hexanediol (Hampton Research), 100 mM MES, pH 6.5. For tetrabutylantimony (TBSb) co-crystallization, 5–10 mM TBSb was added to the well solution before mixing with protein.

Crystal diffraction data collection and analysis

MthK pore crystals were cryo-preserved in liquid N_2 and diffraction data from six crystals with and four without TBSb were collected at 93 K using a wavelength of 1.1 Å at the X25 beamline at the National Synchrotron Light Source, Brookhaven National Laboratory. Their resolution ranged from 1.7 to 2.0 Å. Data were processed using HKL2000 (HKL Research) in space group P1 to reduce noise along the four-fold channel axis and account for the asymmetric TBSb molecule (data can also be processed in $P42_12$, as previously reported[34]). Molecular-replacement phases for these data were determined with Phenix[57] using pdb 3LDC[34] and models were generated through rounds of refinement in Phenix and model building in Coot[58]. All residues fit into the favored region of the Ramachandran plot. Data collection and refinement statistics for two deposited models are given in Table 1. Ordered solvent molecules and ions were previously modeled into densities observed in the MthK pore cavity without blockers (pdb 3LDC). The presence of TBSb (Z = 51) did not result in

the large expected increase in electron density, potentially due to low occupancy. Consequently, we calculated a difference map between the TBSb-containing and TBSb-free data ($F_o^{TBSb} - F_o^{no\text{-}blocker}$) using phases calculated from the TBSb-free structure model (Table 1) with programs from the CCP4 suite[59]. Eleven other difference maps (not shown) also revealed a region of difference density with a maximum peak at 5 – 8 σ located below the selectivity filter. Structural alignment with a model of KcsA with TBA, pdb 2HVK[38], showed the modeled TBA site overlaps with our calculated difference density. The map in Figure 7 was contoured at 4.5 σ in PyMOL. Structural alignment with the published MthK model used for molecular replacement, pdb 3LDC[34], shows the TBSb antimony is located 2.1 Å below an ordered water, modeled below the selectivity filter.

Single-channel recording in lipid bilayers

MthK proteoliposomes were applied to horizontal lipid-decane bilayers (3:1 POPE:POPG in decane) painted across a 100 μm hole in a transparency film partition[33]. The lipid bilayer separated two chambers, *cis* and *trans*, containing recording solutions (190 mM KCl, 10 mM KOH, 10 mM HEPES, pH 8.5 with HCl). 5 mM $CaCl_2$ was added to the *trans* chamber so that only MthK channels with intracellular RCK domains facing *trans* were recorded. Only channels displaying typical behavior such as high open probability and a characteristic current-voltage relationship[33,43] were studied. The most common deviation from typical behavior was a lower maximal Po, observed occasionally. bbTBA was from Spectra Group Limited Inc. Blocker stocks were freshly diluted into recording solution and perfused into *trans* via a gravity-driven solution exchanger. Blocker molecules induced new closed intervals in single-channel recordings, an effect completely reversible. Lipid bilayers were voltage-clamped using the BC-535 bilayer-clamp amplifier (Warner Instruments). Single-channel currents filtered at 2 kHz (4-pole Bessel filter, Warner Instruments), sampled at 25 kHz using a Digidata 1440A (Molecular Devices) were recorded using Axoscope 10.0 software (Molecular Devices).

Single channel kinetic analysis in QuB

Single channel recordings were analyzed using the QuB Classic 2.0.0.9 software (www.qub.buffalo.edu). Curve fits and plots used Origin 6.0 (OriginLab). Current traces were idealized into open and closed dwell-times using the segmental k-means method, which yielded open probabilities (Po) and dwell-time distributions.

Open probability was used to fit the steady-state inactivation data to a Boltzmann equation (Equation 1).

$$P_o = \frac{P_o^{\max}}{1 + e^{\frac{zF(V - V_{1/2})}{RT}}} \quad (1)$$

where P_o^{max} is maximal Po, z is effective valence for inactivation, V is voltage, $V_{½}$ is voltage at half-maximal Po, and RT F^{-1} (gas constant R, temperature T, and Faraday's constant F) is 25.69 at T = 25 °C.

Dwell-time distributions were plotted as log-binned histograms where the ordinate is the square root of the normalized number of events and were used for direct model fitting. Brief closings (flickers) occur at negative voltages and increase in frequency with hyperpolarization. At negative voltages, a QuB dead time was chosen such that flicker gating was fit with one closed state (F). At positive voltages, channel flicker was less frequent (Supplementary Figure 1), and the QuB dead time was adjusted so that channel closings were fit with one closed state (I) that describes voltage-dependent inactivation (Supplementary Figure 1). The dead times were: 0.09 (−125 to −50 mV), 0.18 (−25 mV), 0.5 (25 to 50 mV), and 0.36 (75 to 125 mV) ms. Results were insensitive to these dead-time values. Model fitting in QuB employed a maximum interval likelihood algorithm including a correction for missed events shorter than the dead time[60].

Open-state block was analyzed from −125 to 50 mV with Scheme I (Figure 2b) with no explicit voltage dependence for rates. Transitions between states F and O (channel flicker with rates k_o and k_f) in Scheme I were constrained to no-blocker recording values (Supplementary Figure 1). The second-order blocker on-rate constant k_{on} and the blocker off-rate k_{off} were similar for a model with equal blocker binding to F and O (Supplementary Figure 3), reflecting the insignificance of flicker gating. The voltage dependencies of open-state blocker dissociation constants, $K_D^{open}=k_{off}k_{on}^{-1}$, were analyzed using a model for blocker-K^+ coupling[36] (Equation 2).

$$K_D^{open}(V)=K_D^{low}+K_D^V e^{-\frac{zFV}{RT}} \quad (2)$$

where K_D^{low} is the maximal blocker affinity asymptotically approached at positive voltages, K_D^V is an affinity amplitude for the exponential blocker 'knock-off' term, z is the valence for blocker knock-off.

Open probability was used to determine blocker apparent dissociation constants, K_D^{ap}, during voltage-dependent inactivation (Equation 3).

$$P_o^{blocked}=\frac{P_o^{control}}{1+\frac{[B]}{K_D^{ap}}} \quad (3)$$

where $P_o^{blocked}$ and $P_o^{control}$ are the Po values in the presence and absence of blocker [B].

For channel block and gating kinetic analysis, a single channel was recorded in many experimental conditions (~5 blocker concentrations, from 50 to 125 mV) and globally fit to Schemes IIA, IIB and III (Figure 4a). Rates between states I and O (and IB and OB in Scheme IIB) are voltage dependent, $k_n(V)=k_n e^{\frac{zFV}{RT}}$, where n = 1 to 4, k_n are the rates at 0 mV, and z_n are the valences. Blocker rates, as in Scheme III, include the pseudo first-order block-rates proportional to blocker concentration, $k_{on}[B]$ and $k_{on}^i[B]$, where k_{on} and k_{on}^i are the second-order blocker on-rate constants to the open and inactivated states, respectively. Blocker off-rates are k_{off} and k_{off}^i. State-dependent dissociation constants are

$K_D^{open}=k_{off}k_{on}^{-1}$ and $K_D^{inact}=k_{off}^{i}(k_{on}^{i})^{-1}$. Three independent single channels for TBA (Schemes IIA, IIB, and III), bTBA and bbTBA (Schemes IIA and III only), were analyzed. For tetrapentylammonium (TPA), only one blocker concentration was recorded for 50 to 125 mV, the data were globally fit to Scheme III only, and was repeated for three independent channels. The voltage-dependent inactivation was initially constrained in the global fits to values found for no-blocker experiments (Supplementary Figure 1A). These constraints were then released for finding the best fit. The measured K_D^{ap} values from 50 to 125 mV (Equation 2) were compared to the calculated K_D^{ap} values for Scheme III using mean values for the fit parameters and the following expression (Equation 4, see Supplementary Note for derivation),

$$K_D^{ap}(V)=\frac{\left(1+\frac{k_1}{k_2}e^{\frac{(z_1-z_2)FV}{RT}}\right)K_D^{open}K_D^{inact}}{K_D^{open}+K_D^{inact}\frac{k_1}{k_2}e^{\frac{(z_1-z_2)FV}{RT}}} \quad (4)$$

We also fit the data to a cyclic version of Scheme III that includes voltage-dependent connections between states OB and IB. These additional transitions represent inactivation gating in the presence of bound blocker. However, these rates were not well constrained and were typically fit to values approaching zero (not shown). Since the final conclusion about the gate location is unaltered by this detail, we used Scheme III to describe state-independent blocker access.

Supplementary Material

Refer to Web version on PubMed Central for supplementary material.

Acknowledgments

The authors thank Y. Jiang for advice on MthK crystal preparation and J. Rubin for technical assistance. B. Rothberg (Temple University, Philadelphia, PA) provided the MthK-pQE82 construct. We also thank the staff of the X25 beamline at the National Synchrotron Light Source, Brookhaven National Laboratory for their help. This work was supported by a NRSA postdoctoral fellowship from the National Institutes of Health (F32GM087865) to D.J.P. and a National Institutes of Health grant (RO1GM088352) to C.M.N.

References

1. Hille, B. Ion channels of excitable membranes. Sinauer; Sunderland, Mass: 2001.
2. Armstrong CM, Binstock L. Anomalous Rectification in the Squid Giant Axon Injected with Tetraethylammonium Chloride. J Gen Physiol. 1965; 48:859–72. [PubMed: 14324992]
3. Armstrong CM. Interaction of tetraethylammonium ion derivatives with the potassium channels of giant axons. J Gen Physiol. 1971; 58:413–437. [PubMed: 5112659]
4. Choi KL, Mossman C, Aube J, Yellen G. The internal quaternary ammonium receptor site of Shaker potassium channels. Neuron. 1993; 10:533–41. [PubMed: 8461140]
5. Liu Y, Holmgren M, Jurman ME, Yellen G. Gated access to the pore of a voltage-dependent K+ channel. Neuron. 1997; 19:175–84. [PubMed: 9247273]
6. Holmgren M, Smith PL, Yellen G. Trapping of organic blockers by closing of voltage-dependent K + channels: evidence for a trap door mechanism of activation gating. J Gen Physiol. 1997; 109:527–35. [PubMed: 9154902]

7. Doyle DA, et al. The Structure of the Potassium Channel: Molecular Basis of K+ Conduction and Selectivity. Science. 1998; 280:69–77. [PubMed: 9525859]
8. Zhou M, Morais-Cabral JH, Mann S, MacKinnon R. Potassium channel receptor site for the inactivation gate and quaternary amine inhibitors. Nature. 2001; 411:657–61. [PubMed: 11395760]
9. Jiang Y, et al. Crystal structure and mechanism of a calcium-gated potassium channel. Nature. 2002; 417:515–22. [PubMed: 12037559]
10. Jiang Y, et al. The open pore conformation of potassium channels. Nature. 2002; 417:523–6. [PubMed: 12037560]
11. Yellen G. The moving parts of voltage-gated ion channels. Q Rev Biophys. 1998; 31:239–95. [PubMed: 10384687]
12. Hoshi T, Zagotta WN, Aldrich RW. Biophysical and molecular mechanisms of Shaker potassium channel inactivation. Science. 1990; 250:533–8. [PubMed: 2122519]
13. Kurata HT, Fedida D. A structural interpretation of voltage-gated potassium channel inactivation. Prog Biophys Mol Biol. 2006; 92:185–208. [PubMed: 16316679]
14. Choi KL, Aldrich RW, Yellen G. Tetraethylammonium blockade distinguishes two inactivation mechanisms in voltage-activated K+ channels. Proc Natl Acad Sci U S A. 1991; 88:5092–5. [PubMed: 2052588]
15. McCoy JG, Nimigean CM. Structural correlates of selectivity and inactivation in potassium channels. Biochim Biophys Acta. 2012; 1818:272–85. [PubMed: 21958666]
16. Cuello LG, Jogini V, Cortes DM, Perozo E. Structural mechanism of C-type inactivation in K(+) channels. Nature. 2010; 466:203–8. [PubMed: 20613835]
17. Kurata HT, Wang Z, Fedida D. NH2-terminal inactivation peptide binding to C-type-inactivated Kv channels. J Gen Physiol. 2004; 123:505–20. [PubMed: 15078918]
18. Baukrowitz T, Yellen G. Two functionally distinct subsites for the binding of internal blockers to the pore of voltage-activated K+ channels. Proc Natl Acad Sci U S A. 1996; 93:13357–61. [PubMed: 8917595]
19. Panyi G, Deutsch C. Cross talk between activation and slow inactivation gates of Shaker potassium channels. J Gen Physiol. 2006; 128:547–59. [PubMed: 17043151]
20. Panyi G, Deutsch C. Probing the cavity of the slow inactivated conformation of shaker potassium channels. J Gen Physiol. 2007; 129:403–18. [PubMed: 17438120]
21. Flynn GE, Zagotta WN. Conformational changes in S6 coupled to the opening of cyclic nucleotide-gated channels. Neuron. 2001; 30:689–98. [PubMed: 11430803]
22. Bruening-Wright A, Lee WS, Adelman JP, Maylie J. Evidence for a deep pore activation gate in small conductance Ca2+-activated K+ channels. J Gen Physiol. 2007; 130:601–10. [PubMed: 17998394]
23. Proks P, Antcliff JF, Ashcroft FM. The ligand-sensitive gate of a potassium channel lies close to the selectivity filter. EMBO Rep. 2003; 4:70–5. [PubMed: 12524524]
24. Contreras JE, Srikumar D, Holmgren M. Gating at the selectivity filter in cyclic nucleotide-gated channels. Proc Natl Acad Sci U S A. 2008; 105:3310–4. [PubMed: 18287006]
25. Klein H, et al. Structural determinants of the closed KCa3.1 channel pore in relation to channel gating: results from a substituted cysteine accessibility analysis. J Gen Physiol. 2007; 129:299–315. [PubMed: 17353352]
26. Wilkens CM, Aldrich RW. State-independent block of BK channels by an intracellular quaternary ammonium. J Gen Physiol. 2006; 128:347–64. [PubMed: 16940557]
27. Thompson J, Begenisich T. Selectivity filter gating in large-conductance Ca(2+)-activated K+ channels. J Gen Physiol. 2012; 139:235–44. [PubMed: 22371364]
28. Tang QY, Zeng XH, Lingle CJ. Closed-channel block of BK potassium channels by bbTBA requires partial activation. J Gen Physiol. 2009; 134:409–36. [PubMed: 19858359]
29. Zhou Y, Xia XM, Lingle CJ. Cysteine scanning and modification reveal major differences between BK channels and Kv channels in the inner pore region. Proc Natl Acad Sci U S A. 2011; 108:12161–6. [PubMed: 21730134]
30. Cui J, Yang H, Lee US. Molecular mechanisms of BK channel activation. Cell Mol Life Sci. 2009; 66:852–75. [PubMed: 19099186]

31. Yuan P, Leonetti MD, Hsiung Y, MacKinnon R. Open structure of the Ca2+ gating ring in the high-conductance Ca2+-activated K+ channel. Nature. 2012; 481:94–7. [PubMed: 22139424]
32. Wu Y, Yang Y, Ye S, Jiang Y. Structure of the gating ring from the human large-conductance Ca(2+)-gated K(+) channel. Nature. 2010; 466:393–7. [PubMed: 20574420]
33. Zadek B, Nimigean CM. Calcium-dependent gating of MthK, a prokaryotic potassium channel. J Gen Physiol. 2006; 127:673–85. [PubMed: 16735753]
34. Ye S, Li Y, Jiang Y. Novel insights into K+ selectivity from high-resolution structures of an open K+ channel pore. Nat Struct Mol Biol. 2010; 17:1019–23. [PubMed: 20676101]
35. Thomson AS, Rothberg BS. Voltage-dependent inactivation gating at the selectivity filter of the MthK K+ channel. J Gen Physiol. 2010; 136:569–79. [PubMed: 20937694]
36. Martinez-Francois JR, Lu Z. Intrinsic versus extrinsic voltage sensitivity of blocker interaction with an ion channel pore. J Gen Physiol. 2010; 135:149–67. [PubMed: 20100894]
37. Lenaeus MJ, Vamvouka M, Focia PJ, Gross A. Structural basis of TEA blockade in a model potassium channel. Nat Struct Mol Biol. 2005; 12:454–9. [PubMed: 15852022]
38. Yohannan S, Hu Y, Zhou Y. Crystallographic study of the tetrabutylammonium block to the KcsA K+ channel. J Mol Biol. 2007; 366:806–14. [PubMed: 17196615]
39. Faraldo-Gomez JD, et al. Mechanism of intracellular block of the KcsA K+ channel by tetrabutylammonium: insights from X-ray crystallography, electrophysiology and replica-exchange molecular dynamics simulations. J Mol Biol. 2007; 365:649–62. [PubMed: 17070844]
40. French RJ, Shoukimas JJ. Blockage of squid axon potassium conductance by internal tetra-N-alkylammonium ions of various sizes. Biophys J. 1981; 34:271–91. [PubMed: 7236852]
41. Guo D, Lu Z. Kinetics of inward-rectifier K+ channel block by quaternary alkylammonium ions. dimension and properties of the inner pore. J Gen Physiol. 2001; 117:395–406. [PubMed: 11331349]
42. Spassova M, Lu Z. Coupled ion movement underlies rectification in an inward-rectifier K+ channel. J Gen Physiol. 1998; 112:211–21. [PubMed: 9689028]
43. Pau VP, Abarca-Heidemann K, Rothberg BS. Allosteric mechanism of Ca2+ activation and H+-inhibited gating of the MthK K+ channel. J Gen Physiol. 2010; 135:509–26. [PubMed: 20421375]
44. Woodhull AM. Ionic blockage of sodium channels in nerve. J Gen Physiol. 1973; 61:687–708. [PubMed: 4541078]
45. Thompson J, Begenisich T. External TEA block of shaker K+ channels is coupled to the movement of K+ ions within the selectivity filter. J Gen Physiol. 2003; 122:239–46. [PubMed: 12885878]
46. Heginbotham L, Kutluay E. Revisiting voltage-dependent relief of block in ion channels: a mechanism independent of punchthrough. Biophys J. 2004; 86:3663–70. [PubMed: 15189863]
47. Nimigean CM, Miller C. Na+ block and permeation in a K+ channel of known structure. J Gen Physiol. 2002; 120:323–35. [PubMed: 12198089]
48. Rothberg BS, Shin KS, Phale PS, Yellen G. Voltage-controlled gating at the intracellular entrance to a hyperpolarization-activated cation channel. J Gen Physiol. 2002; 119:83–91. [PubMed: 11773240]
49. Contreras JE, Holmgren M. Access of quaternary ammonium blockers to the internal pore of cyclic nucleotide-gated channels: implications for the location of the gate. J Gen Physiol. 2006; 127:481–94. [PubMed: 16606688]
50. Contreras JE, et al. Voltage profile along the permeation pathway of an open channel. Biophys J. 2010; 99:2863–9. [PubMed: 21044583]
51. Jogini V, Roux B. Electrostatics of the intracellular vestibule of K+ channels. J Mol Biol. 2005; 354:272–88. [PubMed: 16242718]
52. Geng Y, Niu X, Magleby KL. Low resistance, large dimension entrance to the inner cavity of BK channels determined by changing side-chain volume. J Gen Physiol. 2011; 137:533–48. [PubMed: 21576375]
53. Chen X, Aldrich RW. Charge substitution for a deep-pore residue reveals structural dynamics during BK channel gating. J Gen Physiol. 2011; 138:137–54. [PubMed: 21746846]
54. Li W, Aldrich RW. State-dependent block of BK channels by synthesized shaker ball peptides. J Gen Physiol. 2006; 128:423–41. [PubMed: 16966472]

55. Wang DT, Hill AP, Mann SA, Tan PS, Vandenberg JI. Mapping the sequence of conformational changes underlying selectivity filter gating in the K(v)11.1 potassium channel. Nat Struct Mol Biol. 2011; 18:35–41. [PubMed: 21170050]

56. Cuello LG, et al. Structural basis for the coupling between activation and inactivation gates in K(+) channels. Nature. 2010; 466:272–5. [PubMed: 20613845]

57. Adams PD, et al. PHENIX: a comprehensive Python-based system for macromolecular structure solution. Acta Crystallogr D Biol Crystallogr. 2010; 66:213–21. [PubMed: 20124702]

58. Emsley P, Lohkamp B, Scott WG, Cowtan K. Features and development of Coot. Acta Crystallogr D Biol Crystallogr. 2010; 66:486–501. [PubMed: 20383002]

59. Winn MD, et al. Overview of the CCP4 suite and current developments. Acta Crystallogr D Biol Crystallogr. 2011; 67:235–42. [PubMed: 21460441]

60. Qin F, Auerbach A, Sachs F. Estimating single-channel kinetic parameters from idealized patch-clamp data containing missed events. Biophys J. 1996; 70:264–80. [PubMed: 8770203]

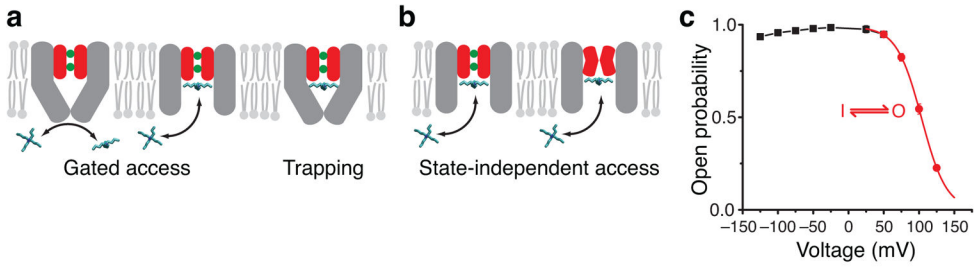

Figure 1.

Block mechanism with two gate locations. (**a**, **b**) MthK pore cartoons illustrating gated access and blocker trapping (**a**) versus state-independent access of blockers (**b**). Selectivity filter is red with two K^+ ions bound (green). Inner-pore helices (grey) may form a bundle-crossing gate. (**c**) Mean open probability (Po) measurements for MthK in symmetric 200 mM K^+ (n = 3–8, mean ± S.D., error bars smaller than symbols). Inactivation gating (50 to 125 mV, red) is described by voltage-dependent transitions between one open (O) and one inactivated (I) state and was fit to a Boltzmann function (red line, Equation 1) with P_o^{max} = 0.994 ± 0.004, z = 1.44 ± 0.02, and $V_{½}$ = 103.3 ± 0.2 mV (Supplementary Figure 1A). The black line has no theoretical meaning.

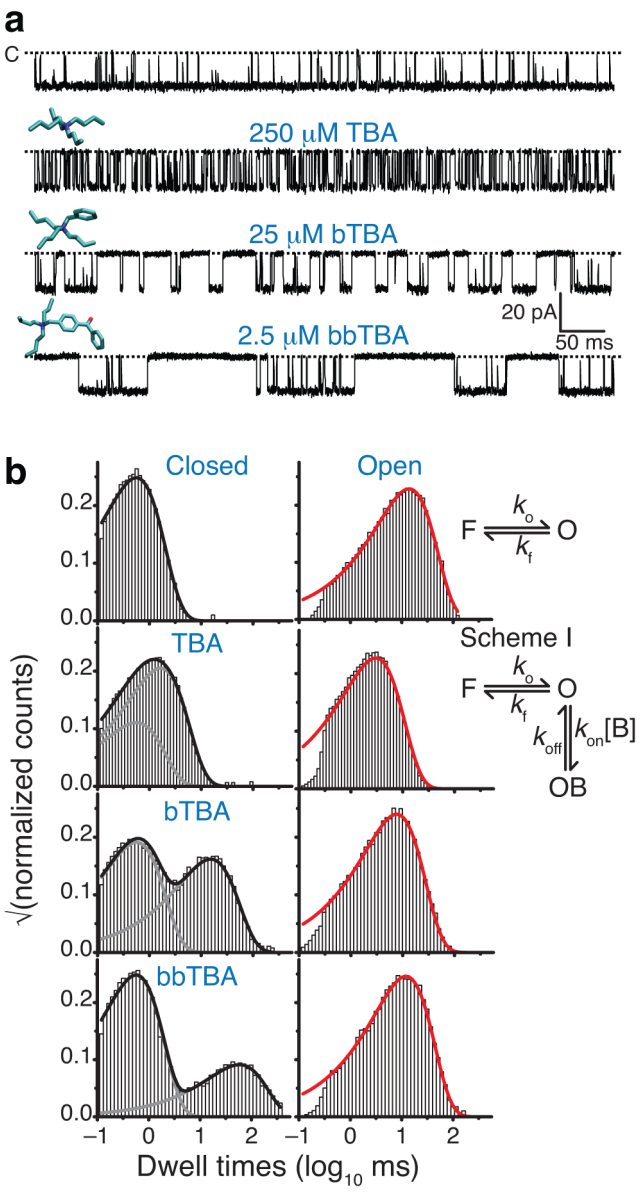

Figure 2.

Block of open MthK. (**a**) Representative recorded currents through single MthK channels at −100 mV with TBA, bTBA, and bbTBA (molecular models shown above traces). Closed level is indicated with a dotted line. (**b**) Closed and open dwell-time distributions for data in **a**. Control (top) was fit to a single closed-open model (right) to fit flicker gating (state F) (Supplementary Figure 1B). Blocker binding was fit with an additional closed state, OB (Scheme I). Fitted rates were used to calculate dissociation constants to MthK open state, $K_D^{open} = k_{off}\, k_{on}^{-1}$. The calculated K_D^{open} values are: TBA, 570 μM; bTBA, 27 μM; and bbTBA, 3.8 μM. Black and red lines are exponential fits to distributions using the schemes (right).

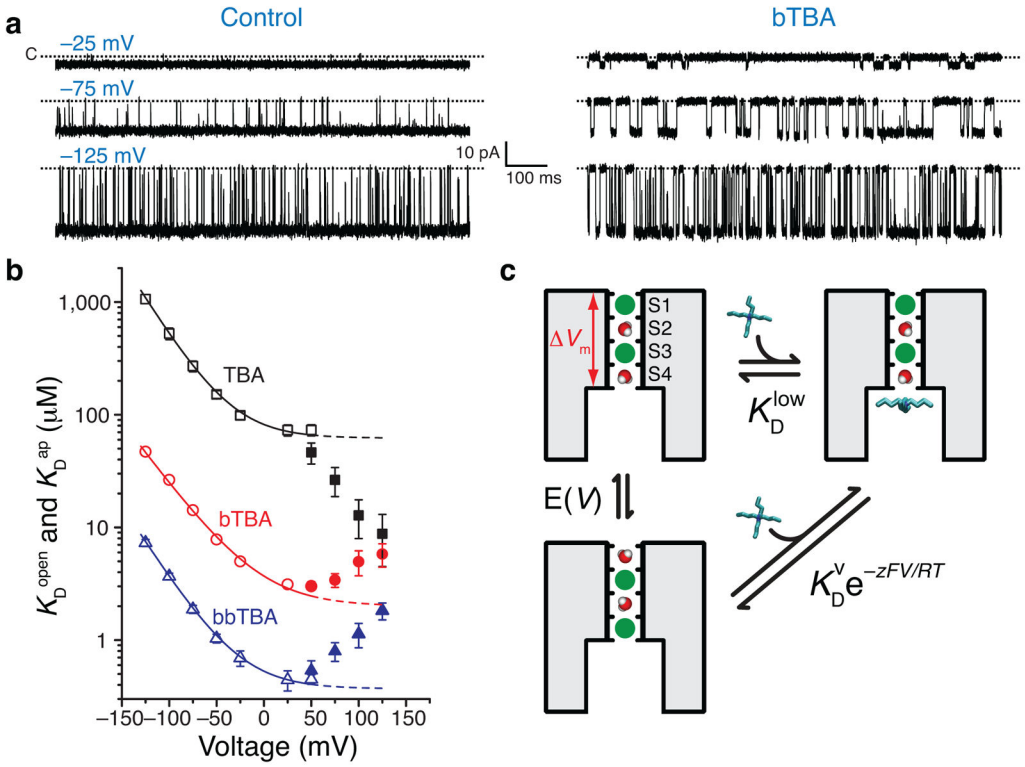

Figure 3.

Voltage dependence of open-state block and apparent affinities during inactivation. (**a**) Single-channel traces without and with 25 μM bTBA at −25, −75, and −125 mV. (**b**) K_D^{open} (open symbols) and K_D^{ap} (filled symbols, Equation 3 for TBA (black squares), bTBA (red circles), and bbTBA (blue triangles), n = 3–6, mean ± S.D., error bars smaller than symbols. K_D^{open} data were fit to a model described in **c** (lines, Equation 2, TBA: K_D^{low} = 62 ± 5 μM, K_D^v = 20 ± 1 μM, z = 0.81 ± 0.01; bTBA: K_D^{low} = 2.0 ± 0.5 μM, K_D^v = 1.7 ± 0.2 μM, z = 0.67 ± 0.03; bbTBA: K_D^{low} = 0.37 ± 0.03 μM, K_D^v = 0.16 ± 0.01 μM, z = 0.78 ± 0.01). Dashed lines are extrapolated K_D^{open} values. (**c**) Cartoon of K^+-blocker coupling model used to fit data in **b** (adapted from ref. 36). Left, pore with two conductive states differing in K^+ (green) distributions in selectivity filter (S1–S3 and S2–S4). Right, TBA (cyan) blocked MthK pore with K^+ in S1–S3. Membrane voltage, ΔV_m, is shown only across selectivity filter. TBA binding with K^+ in S1–S3 is voltage-independent with dissociation constant K_D^{low} (horizontal transition) and TBA binding with K^+ in S2–S4 is voltage-dependent with dissociation constant $K_D^V e^{-\frac{zFV}{RT}}$ (diagonal transition). Cartoon of ion movement between S1–S3 and S2–S4 is a simplification drawn merely for visualization of the ion-coupling concept.

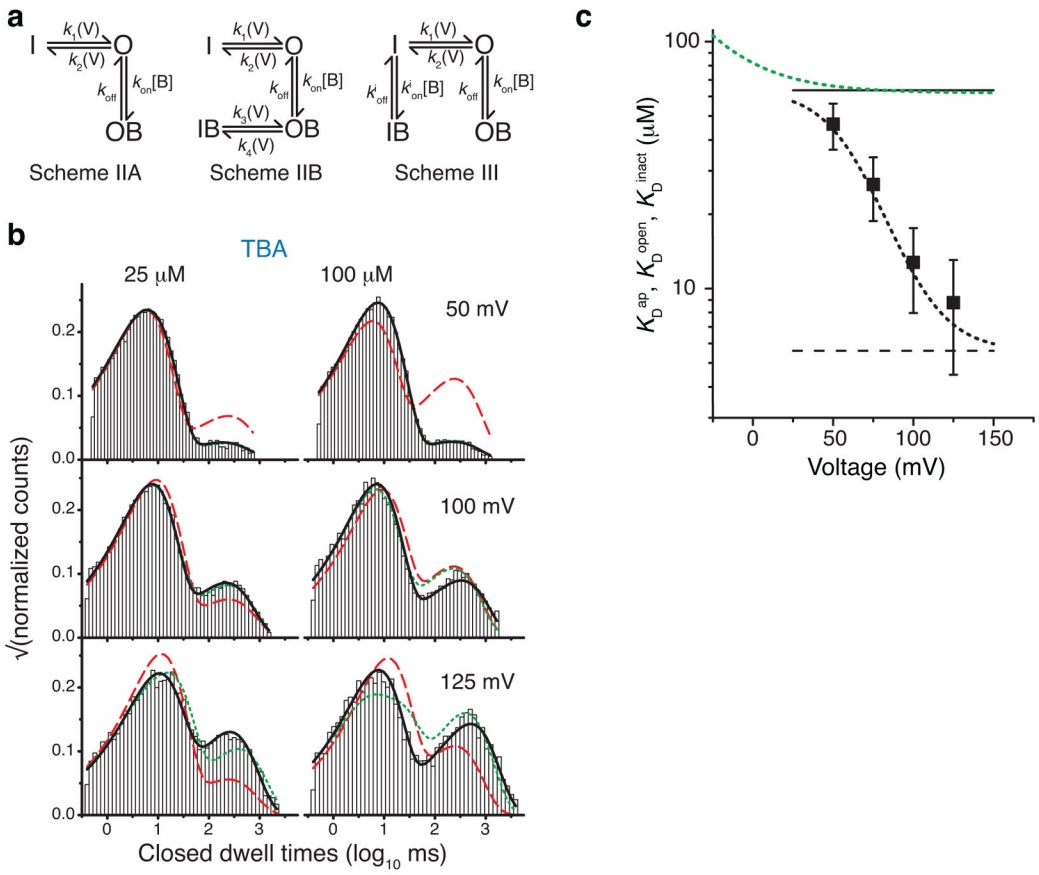

Figure 4.

Inactivation does not gate TBA access to the binding site. (**a**) Schemes used to fit single-channel kinetic data. (**b**) Example closed dwell-time distributions from single MthK recordings with fits to the models in **a**: open channel block (Scheme IIA, red dashed line), blocker trapping (Scheme IIB, green dotted line), and state-independent access models (Scheme III, black line). Fit parameters are in Supplementary Tables (see also Supplementary Figure 4). (**c**) TBA state-independent access (Scheme III) fit results. Black squares are TBA K_D^{ap} measurements from Figure 3 (n = 3–6, mean ± S.D.) and the black dotted line is the predicted K_D^{ap} using fitted parameters with Scheme III (Equation 4, Methods). The green dashed line is the TBA K_D^{open} fit from Figure 3 (Equation 2). The black solid and dashed lines are K_D^{open} (63.5 ± 9.9 μM) and K_D^{inact} (5.6 ± 0.6 μM), respectively, from fits to Scheme III (n = 3, mean ± S.D.).

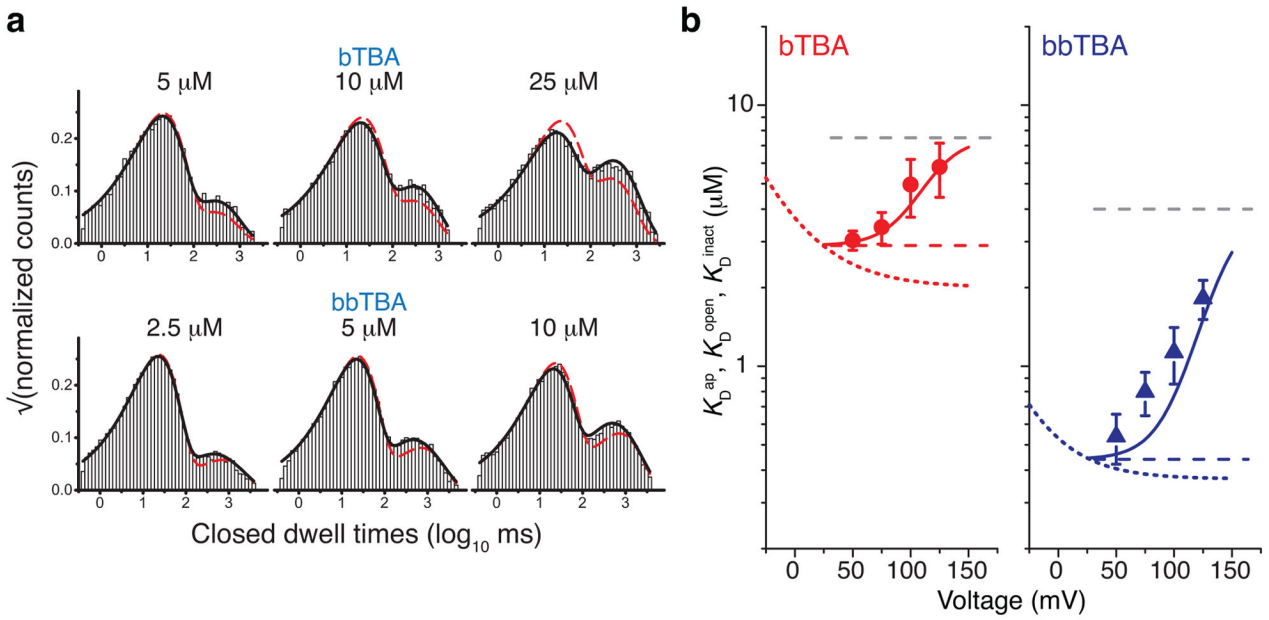

Figure 5.

bTBA and bbTBA block are consistent with state-independent access. (**a**) Example closed dwell-time distributions from single MthK recordings are shown for bTBA (top) and bbTBA (bottom) at 125 mV with fits to the open channel block (Scheme IIA, red dashed line) and the state-independent access (Scheme III, black line) models. Fit parameters are in Supplementary Tables (see Supplementary Figures 5 and 6). (**b**) bTBA (red) and bbTBA (blue) state-independent access (Scheme III) fit results. Red circles (bTBA) and blue triangles (bbTBA) are K_D^{ap} measurements from Figure 3 (n = 3–6, mean ± S.D.) and solid red and blue lines are calculated bTBA and bbTBA K_D^{ap} values using fitted parameters from Scheme III (Equation 4, Methods). Red and blue dotted lines are bTBA and bbTBA K_D^{open} fits from Figure 3 (Equation 2). The red and blue dashed lines are K_D^{open} for bTBA (2.9 ± 0.3 μM) and bbTBA (0.44 ± 0.02 μM), respectively, and grey dashed lines are K_D^{inact} values for bTBA (7.5 ± 1.3 μM) and bbTBA (4.0 ± 0.9 μM) from fits to Scheme III (n = 3, mean ± S.D.).

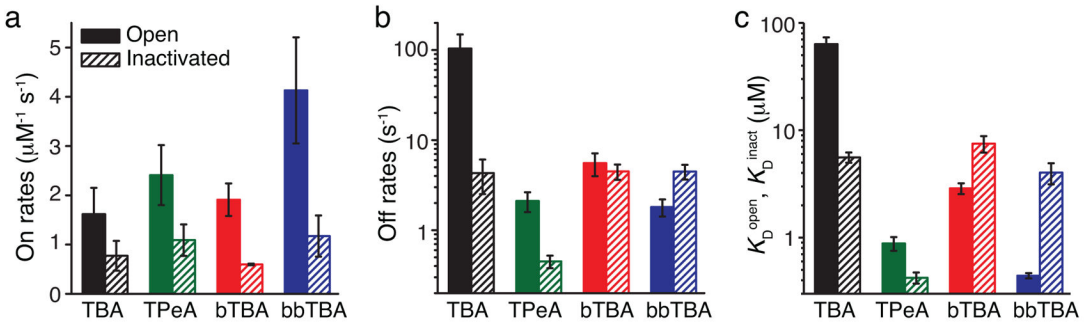

Figure 6.

Summary of state-dependent MthK block. (**a**–**c**) Block kinetics from the state-independent access model (Scheme III) for TBA (black), TPeA (green), bTBA (red), and bbTBA (blue) are plotted for the open state (filled bars) and the inactivated state (dashed bars). Shown are the mean ± S.D. from three fitted datasets (Supplementary Table 3) for blocker on-rate (**a**), off-rate (**b**), and dissociation constants, K_D^{open} and K_D^{inact} (**c**).

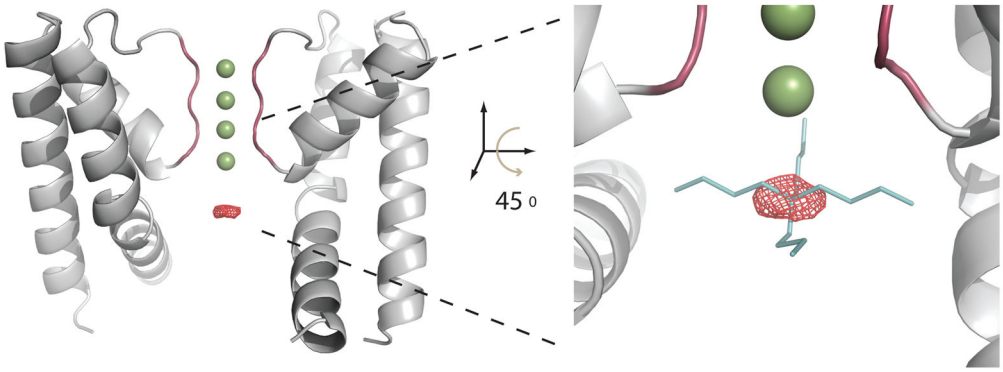

Figure 7.

TBSb difference density in the cavity supports blocker binding immediately below the selectivity filter. Diffraction data for crystals of the isolated MthK pore with and without the heavy TBSb blocker were used to generate a $F_o^{TBSb} – F_o^{no\text{-}blocker}$ difference map (red mesh), shown in the channel cavity, contoured at 4.5 σ. This peak precisely overlapped with a previously modeled TBA molecule (shown right) found in the cavity of KcsA, positioned by aligning the selectivity filter structures of the TBA-KcsA complex (2HVK) with MthK. Two opposing subunits of the MthK channel pore structure are shown in grey with four potassium ions in the selectivity filter (green spheres).

Table 1

Data collection and refinement statistics (molecular replacement)

	MthK	MthK-TBSb
Data collection		
Space group	P1	P1
Cell dimensions		
a, *b*, *c* (Å)	44.03, 63.45, 63.48	43.97, 63.40, 63.48
α, *β*, *γ* (°)	90.03, 89.99, 89.99	89.99, 89.95, 90.00
Resolution (Å)	44.9-1.65 (1.71-1.65) *	44.0-1.70 (1.76-1.70)
R_{sym}	4.2 (39.7)	4.8 (67.7)
$I/\sigma I$	18.7 (2.5)	18.4 (1.8)
Completeness (%)	96.3 (93.8)	96.4 (93.2)
Redundancy	3.2 (3.0)	3.3 (3.1)
Refinement		
Resolution (Å)	44.86-1.65	36.14-1.69
No. reflections	78558	73246
R_{work}/R_{free}	0.164/0.181	0.173/0.191
No. atoms		
Protein	5240	5224
Ligand/ion	104	168
Water	266	216
B-factors		
Protein	21.8	29.8
Ligand/ion	47.6	58.2
Water	33.3	39.4
R.m.s. deviations		
Bond lengths (Å)	0.010	0.009
Bond angles (°)	1.173	1.112

* Values in parentheses are for highest-resolution shell.